RSC Advances

ROYAL SOCIETY OF CHEMISTRY

www.rsc.org/advances

C-doped boron nitride fullerene as a novel catalyst for acetylene hydrochlorination: a DFT study

Fei Zhao, Yang Wang, Mingyuan Zhu, Lihua Kang*

College of Chemistry and Chemical Engineering/ Key Laboratory for Green Processing of Chemical Engineering of Xinjiang Bingtuan. Shihezi University, Shihezi, Xinjiang, 832000, PR China

Abstract: Density functional theory calculations were used to investigate the mechanism of acetylene hydrochlorination separately catalyzed by un-doped $B_{12}N_{12}$ and carbon-doped BN fullerene ($B_{12-n}N_{11+n}C$ (n = 0, 1)). We have discovered that carbon-doped BN clusters displayed extraordinary catalyst performance for acetylene hydrochlorination compared with un-doped $B_{12}N_{12}$ clusters. C_2H_2 was adsorbed onto $B_{12-n}N_{11+n}C$ (n = 0, 1) clusters prior to HCl and then formed three adsorption states. The first two states were trans configuration, in which the two H atoms of C_2H_2 were on opposite sides of the C=C bond; the third state was cis configuration, in which the two H atoms were on the same side of the C=C bond. Afterwards, we illustrated three possible pathways with corresponding transition states. In particular, the minimum energy pathway R1 based on the $B_{11}N_{12}C$ catalyst had an energy barrier as low as 36.08 kcal·mol^{-1}, with only one transition state.

Keywords: C-doped BN fullerene, acetylene hydrochlorination, reaction mechanism, trans-form adsorb, DFT

*Corresponding author.E-mail: kanglihua@shzu.edu.cn

Tel: +86-0993-2057213; Fax: +86-0993-2057270

1. Introduction

Not long after the discovery of C_{60} by Kroto et al. in 1985[1], research on fullerene and related materials boomed. Because the first case of successful preparation of doped fullerene[2], investigators have extensively researched the preparation, structure, and application of various doped fullerenes[3-11]. Among these doped fullerenes, the $B_{12}N_{12}$ cage is considered to be the smallest stable cage [6, 12, 13]. $B_{12}N_{12}$ cages were successfully synthesized by Oku et al. in 2004 and were analyzed by laser desorption time-of-flight mass spectrometry [6, 14]. Their research revealed that $B_{12}N_{12}$ clusters consisting of four- and six-membered BN rings satisfy the isolated tetragonal rule. Although scientists have widely explored the usage of these clusters as catalysts, many studies have concentrated on their application as hydrogen-storage materials [8, 9, 15, 16] and have neglected their potential roles in other reactions. In the present work, doped BN fullerene was used as a catalyst for acetylene hydrochlorination for the first time.

Mercuric chloride is the most commonly used catalyst for the industrial production of vinyl chloride monomer. However, mercuric chloride catalyst easily sublimes at high temperatures [17, 18] and seriously harms human health and the environment. Therefore, possible alternatives that are efficient and environment friendly are necessary. In 1985[19], Hunchings et al. predicted that gold-based catalysts could be greener

substitutes for mercuric chloride. They performed an experiment[20] to confirm that Au^{3+} possesses the highest catalytic activity among the selected metal complexes containing Bi^{3+} [21], Pd^{2+} [22], Pt^{2+} [23], and Pt^{4+} [24]. However，the supported gold catalysts were more easily deactivated with prolonged reaction time because the active gold species Au^{3+} is reduced to Au^{0} [25]. To overcome this difficulty, J. Zhang et al. studied the deactivation mechanism of $AuCl_3$ catalyst through the $AuCl_3$ dimer model and density functional theory (DFT)[26]. M. Zhu et al. developed various methods to enhance the activation and stability of Au^{3+} by preparing $AuCl_3$/PPy–MWCNTs catalysts [27-29]. L. Kang et al. investigated the reaction mechanism of the hydrochlorination of acetylene to C_2H_3Cl over MCl_x (M = Hg, Au, Ru; x = 2, 3) catalyst. They concluded that $RuCl_3$ could be a good candidate catalyst based on theoretical calculations[30]. Other scientists have researched the mechanisms, active sites, and deactivation [31-33]. Most of the reported studies are focused on metal chloride catalysts [34-38], and research on non-metallic catalysts, especially C-doped BN cages, for acetylene hydrochlorination is limited [39-43].

In the present study, DFT was used to study the adsorption and dissociation of C_2H_2 and HCl on un-doped $B_{12}N_{12}$ and C-doped $B_{12-n}N_{11+n}C$ (n = 0, 1) cages, respectively. The mechanisms of acetylene hydrochlorination to vinyl chloride catalyzed by BNC ($B_{12-n}N_{11+n}C$ (n = 0, 1)) cages were examined. These investigations on the reaction mechanism

of acetylene hydrochlorination on BN cages can aid the design of new environmentally benign, non-mercury catalysts and facilitate the sustainable development of the polyvinyl chloride industry.

2. Computational methods

All DFT calculations were executed using the Guassian09 program package [44]. No symmetry constraints were imposed on the geometry optimization. The hybrid density functionals of Lee, Yang and Parr (B3LYP)[45] with the 6-31+G** basis set were applied for all structures, including reactants, products, intermediates, and transition states. All stationary points mentioned were characterized as minima (no imaginary frequency) or transition states (one imaginary frequency) through a Hessian calculation. Intrinsic reaction coordinate (IRC) [46, 47] calculations were performed to confirm that the reaction links the correct products to the reactants. Transition-state structures were characterized using frequency calculations and by analyzing the vibrational modes. In all instances, only one imaginary frequency corresponding with the reaction coordinate was obtained. Basis set superposition error[48] corrections evaluated by the counterpoise method were considered.

Considering frontier molecular orbital (FMO) and charge-distribution analysis, we can estimate the approximate distribution of the active sites of the BNC cages, as well as the highest occupied molecular orbital (HOMO) and the lowest unoccupied molecular orbital (LUMO) energies

of the C_2H_2, HCl, and BNC cages. By calculating the HOMO-LUMO energy gaps, we obtained the lowest HOMO-LUMO energy gaps and ascertained the electron donor and acceptor. We have further verified the predicted consequence of FMO analysis through charge-distribution analysis.

3. Results and discussion

3.1 Geometries of reactants and adsorption onto BNC cages

3.1.1 Geometries of reactants

The reactants included isolated C_2H_2 molecules, HCl molecules, un-doped $B_{12}N_{12}$, and the corresponding C-doped $B_{12-n}N_{11+n}C$ (n = 0, 1) cages. Figure 1 displays the optimized structure of the reactants. The $B_{12}N_{12}$ cage is the smallest stable BN fullerene among all known BN cages [3, 6]. All B or N sites are equivalent with Th symmetry for cages composed of alternately distributed boron and nitrogen atoms. Considering this cage from a structure perspective, the $B_{12}N_{12}$ cage (shown in Figure 1(a)) is composed of six 4-membered rings (4-MR) and eight 6-membered rings (6-MR). The B-N bonds were of two types: one was shared by two adjacent 6-MRs with the lengths of 1.439 Å, and the other was shared by a 4-MR and a 6-MR with lengths of 1.487 Å. The charges were uniformly distributed on the $B_{12}N_{12}$ cage with a Mulliken value of 0.57 for B atoms and -0.57 for N atoms.

By separately substituting one C atom for a B or N atom in $B_{12}N_{12}$,

$B_{11}N_{12}C$ and $B_{12}N_{11}C$ were obtained. As shown in the HOMO in Figure 2(b), electrons accumulated around the C1 atom in $B_{11}N_{12}C$, as well as in $B_{12}N_{11}C$ (Figure 2(c)). The charges of the C1 atom in $B_{11}N_{12}C$ and $B_{12}N_{11}C$ were -0.812 and -0.023, respectively. As a result, C-doping lengthened the adjacent C1-N3 bond from 1.439 Å to 1.418 Å (Figure 1(b)) and the C1-B3 bond to 1.546 Å in $B_{12}N_{11}C$ (Figure 1(c)), which made the C1 atom appear slightly embossed. The Mulliken charges of the C1 atom were -0.81 in $B_{11}N_{12}C$ and -0.023 in $B_{12}N_{11}C$. The C1 site was more active than any other site in the cages.

3.1.2 Adsorption of acetylene and hydrogen chloride onto BNC cages

Figure 5 and Table 2 illustrate the weak adsorption of C_2H_2 and HCl onto the $B_{12}N_{12}$ cage. In Figure 5, the distance between the adsorbate and the $B_{12}N_{12}$ cage was longer than 2 Å, reaching more than 3 Å for C_2H_2. Moreover, neither obvious change in bond length nor distortion in shape of the $B_{12}N_{12}$ cage and adsorbate was observed, indicating that C_2H_2 and HCl molecules were physically adsorbed onto the $B_{12}N_{12}$ cage. The adsorption energies (E_{ad}) were calculated by equation (1).

$$E_{ad} = E_{adsorption\ state} - \left(E_{reactant} + E_{catalyst}\right) \qquad (1)$$

Table 2 shows the adsorption energies of C_2H_2 and HCl on the nanocages. The adsorption energies of C_2H_2 and HCl onto $B_{12}N_{12}$ were very low, suggesting that C_2H_2 and HCl cannot stably adsorb onto the $B_{12}N_{12}$ cage and be efficiently activated by catalyst.

Table 1 and Figure 3 list the orbital energies of the HOMOs and LUMOs of C_2H_2, HCl, $B_{12}N_{12}$, $B_{11}N_{12}C$, and $B_{12}N_{11}C$, as well as their energy gaps. The energy gaps of the HOMO-LUMO (C_2H_2→BNC) were smaller than those of the HOMO-LUMO (BNC→C_2H_2), indicating that C_2H_2 was an electron donor. In contrast to C_2H_2, the energy gaps of HOMO-LUMO (HCl→BNC) were larger than those of HOMO-LUMO (BNC→HCl), indicating that HCl was an electron acceptor. The energy gaps represented the ability of electrons to transfer from C_2H_2/HCl to the BNC cages. Figure 3 clearly shows that the energy gaps of HOMO-LUMO (C_2H_2→BNC) were smaller than those of HOMO-LUMO (HCl→BNC). Thus, we can predict that acetylene was better adsorbed onto the BNC cages than HCl, as verified by comparing adsorption energies.

The corresponding adsorption energies of C_2H_2 and HCl adsorbed onto BNC cages are displayed in Figure 4. Besides, Table 2 lists the optimal adsorption energies of C_2H_2 and HCl onto the BNC cages. We can clearly observe that C_2H_2 was more easily adsorbed onto BNC than HCl, which confirmed the previous prediction obtained by the HOMO-LUMO energy gaps. These cages primarily adsorbed C_2H_2 to form BNC-C_2H_2 complexes, which subsequently adsorbed HCl because of the considerable difference in the adsorption energies of C_2H_2 and HCl. This conclusion was the same as that drawn from the HOMO-LUMO energy

gap analysis.

To identify the most favorable adsorption configurations on the $B_{11}N_{12}C$ and $B_{12}N_{11}C$ cages, a C_2H_2 molecule was originally placed in different sites on the surface of the nanocages with different directions. We obtained the three most stable single-component adsorption configurations (A, B, and C), as shown in Figure 5. A and B corresponds to a C_2H_2 molecule adsorbed onto a $B_{11}N_{12}C$ cage, and C was corresponds to a C_2H_2 molecule adsorbed onto a $B_{12}N_{11}C$ cage. Figures 5(A and B) show that the C_2H_2 adsorbed onto the $B_{11}N_{12}C$ cage in a different way, i.e., in the trans configuration for A and in the cis configuration for B. This subtle distinction considerably influenced the mechanism, as elaborated in the next part. Given that the π molecular orbital of C_2H_2 transferred to the BNC cages, the C≡C triple bond became a double bond, and the bond length increased from 1.208 Å to 1.312, 1.312, and 1.317 Å. A C–C single bond formed between the C2 atom of acetylene and the C1 atom of the BNC cage, and the bond lengths were 1.513, 1.506, and 1.517 Å, respectively. More distortions were observed in the angles of the C_2H_2 molecule, which revealed that C_2H_2 molecular was well-activated. These results further demonstrated that C-doped $B_{12-n}N_{11+n}C$ (n = 0, 1) fullerenes had considerable sorption capacity and that the C1 site had high activity.

3.2 Reaction mechanisms of acetylene hydrochlorination over BNC cages

The possible reaction pathways were systematically examined to gain a better understanding of the reaction mechanism of $B_{11}N_{12}C$ and $B_{12}N_{11}C$ catalyzing the reaction of acetylene hydrochlorination. Figure 6 shows the reaction pathways starting from HCl and C_2H_2 co-adsorption structures (Figure 5(A, B, and C)) denoted as R1, R2, and R3, respectively. The structures of the various stationary points located on the potential energy surface are depicted in Figures 7–9, along with the values of the most relevant geometrical parameters.

3.2.1 Reaction mechanism of R1

The reaction pathway started with the structure of C_2H_2 adsorbing onto $B_{11}N_{12}C$, as shown in Figure 5(A). The adsorption configurations were of two types, i.e., cis- and trans-adsorption structures. The co-adsorption energy of the former was -28.39 kcal·mol^{-1}, which was slightly higher than the -28.45 kcal·mol^{-1} of the latter. Accordingly, we considered that the trans-form resulted in a shorter reaction pathway and a significantly lower activation barrier of 36.08 kcal·mol^{-1} in pathway 1 than the 49.63 kcal·mol^{-1} in pathway 2. Therefore, only one transition state existed for pathway 1.

The HCl molecule subsequently adsorbed onto the C_2H_2-$B_{11}N_{12}C$ complex to form a co-adsorption configuration. Considering the changes in the bond length and adsorption energy, HCl was nearly unactivated in the co-adsorption state. The co-adsorption structure can be converted into

the de-adsorption structure through the transition state Ts1 (Figure 7). In the Ts1 state, the HCl molecule shifted to the other side of the C=C double bond and closer to the C=C double bond. Meanwhile, the bond length of H–Cl increased from 1.306 Å to 1.877 Å compared with the co-adsorption state. The H1 atom approached the C2 atom, and the distance between them decreased to 1.355 Å. This finding proved that the HCl molecule completely dissociated and was activated in the Ts1 state. Only one imaginary frequency (-1090.30 cm^{-1}) was obtained from the vibrational analysis of the Ts1 structure. This frequency was associated with the stretching movement of the H1 atom. To achieve the Ts1 state, a climb over the energy barrier of 36.08 $kcal \cdot mol^{-1}$ (the activation energy of acetylene hydrochlorination) was required. This step was the rate-limiting step. To evaluate the catalyst activity of $B_{11}N_{12}C$ in acetylene hydrochlorination, we compared the energy barrier in the rate-limiting step on $B_{11}N_{12}C$ with other calculated non-metal catalysts (Table 3). The results showed that $B_{11}N_{12}C$ performed well.

To gain a better understanding of the reaction mechanism, an IRC calculation was performed to confirm that the transition state structure linked the co-adsorption complex to the de-adsorption complex. No further intermediates were involved in the reactions. In the de-adsorption state, the target product C_2H_3Cl molecule adsorbed onto $B_{11}N_{12}C$ cages to form adsorption complexes. The bond length of the calculated C2–C3

was 1.488 Å, longer than the 1.329 Å of the free C_2H_3Cl molecule. The final step was the desorption of C_2H_3Cl molecules, and the desorption energy was 25.41 kcal·mol^{-1}, which was equal to the adsorption energy of the C_2H_3Cl molecule onto the $B_{11}N_{12}C$ cage.

3.2.2 Reaction mechanism of R2 and R3

In view of the resemblance between the mechanisms of R2 and R3 (Figures 8 and 9), we combined the two mechanisms for simplicity of explanation. Similar to R1, the C_2H_2 molecule was firstly chemisorbed onto the $B_{11}N_{12}C$ and $B_{12}N_{11}C$ cages, and then the HCl molecule continued to adsorb onto the C_2H_2-$B_{11}N_{12}C$ and C_2H_2-$B_{12}N_{11}C$ complexes to form co-adsorption structures. However, they physically adsorbed onto the complexes because of the weak interaction between the HCl molecule and the C-doped BN cage. The bond lengths of C1–C2, C2–C3, and H1–Cl were only very slightly changed, further confirming that HCl was unactivated.

The structure of co-adsorption can change to Ims1 with transition state Ts1. In this structure, the H1–Cl bond was substantially lengthened and induced the elimination of thee HCl molecule. The H1–Cl bond length increased from 1.302 Å to 1.517 Å compared with the co-adsorption state in R2. A significant change in the coordination of the HCl molecule also occurred. The Cl atom approached the C2 site in R2, and the distance between them decreased from 3.647 to 1.988 Å compared with the

co-adsorption state, indicating that HCl was completely activated. We observed an interesting phenomenon about the Ts1 state (Figure 9) in R3. The H–Cl bond was not only broken but also nearly adsorbed in parallel onto the C=C bond and formed a dihedral angle of 0.883 between the H1–Cl and C2–C3 atoms. At the same time, the H–Cl bond length increased from 1.306 Å to 1.552 Å, but the other critical bonds, such as C1–C2 and C2–C3, underwent only very slight changes.

The only imaginary frequency (-2480 cm^{-1} in R2 and -1780.75 cm^{-1} in R3) was obtained from the vibrational analysis of the Ts1 structure. This phenomenon was associated with the stretching movement of the H1 atom. To achieve the Ts1 state, a climb over the energy barriers of 49.63 and 41.41 $kcal \cdot mol^{-1}$ (the activation energy of acetylene hydrochlorination) was required. This step was the rate-controlling step for both pathways.

To gain a better understanding of the reaction mechanism, an IRC calculation was performed for co-adsorption conversion to Ims1. The IRC calculation confirmed that the Ts1 state linked the co-adsorption and Ims1 states. In the Ims1 state, a C3–Cl bond was formed by the attraction of the C3 atom. Figures 8 and 9 show that the HCl molecule dissociated in Ts1, and the Cl atom and the nearest C3 atom had opposite charges. The charges of the Cl atom were 0.089 in R2 and 0.129 in R3. The C3 atom had opposite charges of -0.163 in R2 and -0.070 in R3. The interaction

between the opposite charges caused the chlorine atom to transfer from HCl to the C3 site of the C_2H_2-$B_{11}N_{12}C$ complex to form a C3–Cl bond in the Ims1 state. The distance between the C3 and Cl atom decreased from 1.988 Å to 1.745 Å in R2 and 1.753 Å in R3 compared with the Ts1 state.

The intermediate state Ims1 can generate a de-adsorption product with transition state Ts2. In the Ts2 state of both pathways, the H1 atom that separated from the HCl molecule almost perpendicularly approached the C2 site. The distance between the C2 and H1 atoms was 2.169 Å in R2 and 2.09 Å in R3. The only imaginary frequency (475.15 cm^{-1} in R2 and -459.88 cm^{-1} in R3) was obtained from the vibrational analysis of the Ts2 structure, which was associated with the stretching movement of the H1 atom. To obtain the Ts2 state of R2, the Ims1 state required climbing over an energy barrier of only 1.4 $kcal \cdot mol^{-1}$. The corresponding energy barrier of R3 was 1.34 $kcal \cdot mol^{-1}$. Thus, the H1 atom was easily attracted by the C_2H_2Cl- $B_{12-n}N_{11+n}C$ (n = 0, 1) complex.

IRC calculation was performed again to confirm that the Ts2 state can convert into the de-adsorption state, in which the target product C_2H_3Cl molecule adsorbed onto $B_{12-n}N_{11+n}C$ (n = 0, 1) cages to form adsorption complexes. In spite of the different adsorption configurations in R1 and R2, the same de-adsorption configuration was formed. In the de-adsorption state of R3, the bond length of the calculated C2–C3 was 1.489 Å, longer than 1.329 Å in the free C_2H_3Cl molecule. The final step

was the desorption of the C_2H_3Cl molecule, and the desorption energy in R3 was 23.98 kcal·mol^{-1}, which was equal to the adsorption energy of the C_2H_3Cl molecule adsorbed onto the $B_{12}N_{11}C$ cage.

4. Conclusions

According to our DFT calculations at the B3LYP/6-31+G** level, the doping of C atoms on the BN cages can significantly intensify the adsorption ability of the C_2H_2 molecule compared with the un-doped BN cages. The first step of the reaction was C_2H_2 adsorption, and the rate-limiting step was the dissociation of the HCl molecule in the TS1 state. In addition, we found that the trans-adsorption of the C_2H_2 molecule on the $B_{11}N_{12}C$ cage was more favorable for acetylene hydrochlorination than cis-adsorption. Trans-adsorption can efficiently reduce the activation barrier and shorten the reaction pathway. The energy barrier for H1–Cl scission in pathway R1 was much lower than those in R2 and R3, suggesting that acetylene hydrochlorination much more easily occurred than in R1 and R3. Our investigations indicated that $B_{11}N_{12}C$ performed well among non-metal catalysts and can be a candidate catalyst for acetylene hydrochlorination. We hope that our results can be useful for designing and developing novel nonmetallic catalysts.

Acknowledgments

We gratefully acknowledge the National Natural Science Fundation of

China (NSFC, Grant No. 11304208) and the Science and Technology Fund Projects of Shihezi University (No. 2014ZRKXJQ03).

References

1 H. Kroto, R. E. Smalley and J. Heath, *Nature*, 1985, **318**, 162-163.

2 T. Guo, C. Jin and R. E. Smalley, *The Journal of Physical Chemistry*, 1991, **95**, 4948-4950.

3 F. Jensen and H. Toftlund, *Chemical Physics Letters*, 1993, **201**, 89-96.

4 D. L. Strout, *The Journal of Physical Chemistry A*, 2000, **104**, 3364-3366.

5 H. Wu, X. Xu, H. Jiao, F. Zhang and J. Jia, *Chinese Science Bulletin*, 2003, **48**, 1102.

6 T. Oku, A. Nishiwaki and I. Narita, *Science and Technology of Advanced Materials*, 2004, **5**, 635-638.

7 M. D. Esrafili and R. Nurazar, *Superlattices and Microstructures*, 2014, **67**, 54-60.

8 T. Oku, M. Kuno and I. Narita, *J Phys Chem Solids*, 2004, **65**, 549-552.

9 M. D. Esrafili and R. Nurazar, *Computational Materials Science*, 2014, **92**, 172-177.

10 T. Oku, *Energies*, 2015, **8**, 319-337.

11 A. Soltania, M. T. Baei, E. T. Lemeski and M. Shahini, *Superlattices And Microstructures*, 2014, **76**, 315-325.

12 G. Seifert, P. W. Fowler, D. Mitchell, D. Porezag and T. Frauenheim,

Chemical Physics Letters, 1997, **268**, 352-358.

13 W. H. Moon, M. S. Son and H. J. Hwang, *Applied surface science*, 2007, **253**, 7078-7081.

14 T. Oku, T. Hirano, M. Kuno, T. Kusunose, K. Niihara and K. Suganuma, *Materials Science and Engineering: B*, 2000, **74**, 206-217.

15 H. Wu, X. Fan and J. Kuo, *International Journal of Hydrogen Energy*, 2012, **37**, 14336-14342.

16 H. Wu, X. Fan, J. Kuo and W. Deng, *Chemical communications*, 2010, **46**, 883-885.

17 G. J. Hutchings and D. T. Grady, *Applied Catalysis*, 1985, **16**, 411-415.

18 G. J. Hutchings and D. T. Grady, *Applied Catalysis*, 1985, **17**, 155-160.

19 G. J. Hutchings, *Journal of Catalysis*, 1985, **96**, 292-295.

20 B. Nkosi, N. J. Coville and G. J. Hutchings, *J. Chem. Soc., Chem. Commun.*, 1988, 71-72.

21 X. Wei, F. Wei, W. Qian, G. Luo, H. Shi and Y. Jin, *The Chinese Journal of Process Engineering*, 2008, **6**, 034.

22 Q. Song, S. Wang, B. Shen and J. Zhao, *Petroleum Science and Technology*, 2010, **28**, 1825-1833.

23 U. Dzhemilev, O. Vostrikova and G. Tolstikov, *AE Shilov, Gordon and Breach, New York*, 1986, **2**.

24 S. A. Mitchenko, E. V. Khomutov, A. A. Shubin and Y. M. Shul'ga, *Journal of Molecular Catalysis A: Chemical*, 2004, **212**, 345-352.

25 B. Nkosi, M. D. Adams, N. J. Coville and G. J. Hutchings, *Journal of Catalysis*, 1991, **128**, 378-386.

26 J. Zhang, Z. He, W. Li and Y. Han, *RSC Advances*, 2012, **2**, 4814-4821.

27 X. Li, M. Zhu and B. Dai, *Applied Catalysis B: Environmental*, 2013, **142–143**, 234-240.

28 C. Huang, M. Zhu, L. Kang and B. Dai, *Catalysis Communications*, 2014, **54**, 61-65.

29 C. Huang, M. Zhu, L. Kang, X. Li and B. Dai, *Chemical Engineering Journal*, 2014, **242**, 69-75.

30 M. Zhu, L. Kang, Y. Su, S. Zhang and B. Dai, *Canadian Journal of Chemistry*, 2013, **91**, 120-125.

31 M. Conte, A. F. Carley, C. Heirene, D. J. Willock, P. Johnston, A. A. Herzing, C. J. Kiely and G. J. Hutchings, *Journal of catalysis*, 2007, **250**, 231-239.

32 K. Zhou, W. Wang, Z. Zhao, G. Luo, J. T. Miller, M. S. Wong and F. Wei, *ACS Catalysis*, 2014, **4**, 3112-3116.

33 M. Conte, A. F. Carley, G. Attard, A. A. Herzing, C. J. Kiely and G. J. Hutchings, *Journal of Catalysis*, 2008, **257**, 190-198.

34 J. Ma, S. Wang and B. Shen, *Reaction Kinetics, Mechanisms and*

Catalysis, 2013, **110**, 177-186.

35 S. Wang, B. Shen and Q. Song, *Catalysis Letters*, 2009, **134**, 102-109.

36 J. Zhao, X. Cheng, L. Wang, R. Ren, J. Zeng, H. Yang and B. Shen, *Catalysis Letters*, 2014, **144**, 2191-2197.

37 J. Zhao, J. Zeng, X. Cheng, L. Wang, H. Yang and B. Shen, *RSC Adv.*, 2015, **5**, 16727-16734.

38 K. Zhou, J. Jia, C. Li, H. Xu, J. Zhou, G. Luo and F. Wei, *Green Chem.*, 2015, **17**, 356-364.

39 X. Li, Y. Wang, L. Kang, M. Zhu and B. Dai, *Journal of Catalysis*, 2014, **311**, 288-294.

40 B. Dai, K. Chen, Y. Wang, L. Kang and M. Zhu, *ACS Catalysis*, 2015, **5**, 2541-2547.

41 X. Wang, B. Dai, Y. Wang and F. Yu, *ChemCatChem*, 2014, **6**, 2339-2344.

42 K. Zhou, B. Li, Q. Zhang, J. Q. Huang, G. L. Tian, J. C. Jia, M. Q. Zhao, G. H. Luo, D. S. Su and F. Wei, *ChemSusChem*, 2014, **7**, 723-728.

43 K. Zhou, J. Si, J. Jia, J. Huang, J. Zhou, G. Luo and F. Wei, *RSC Advances*, 2014, **4**, 7766-7769.

44 M. J. Frisch, G. W. Trucks, H. B. Schlegel, G. E. Scuseria, M. A. Robb, J. R. Cheeseman, G. Scalmani, V. Barone, B. Mennucci, G. A. Petersson, H. Nakatsuji, M. Caricato, H. P. H. X. Li, A. F. Izmaylov, J.

Bloino, G. Zheng, J. L. Sonnenberg, M. Hada, M. Ehara, K. Toyota, R. Fukuda, J. Hasegawa, M. Ishida, T. Nakajima, Y. Honda, O. Kitao, H. Nakai, T. Vreven, J. A. Montgomery, Jr., J. E. Peralta, F. Ogliaro, M. Bearpark, J. J. Heyd, E. Brothers, K. N. Kudin, V. N. Staroverov, T. Keith, R. Kobayashi, J. Normand, K. Raghavachari, A. Rendell, J. C. Burant, S. S. Iyengar, J. Tomasi, M. Cossi, N. Rega, J. M. Millam, M. Klene, J. E. Knox, J. B. Cross, V. Bakken, C. Adamo, J. Jaramillo, R. Gomperts, R. E. Stratmann, O. Yazyev, A. J. Austin, R. Cammi, C. Pomelli, J. W. Ochterski, R. L. Martin, K. Morokuma, V. G. Zakrzewski, G. A. Voth, P. Salvador, J. J. Dannenberg, S. Dapprich, A. D. Daniels, O. Farkas, J. B. Foresman, J. V. Ortiz, J. Cioslowski and D. J. Fox, *Gaussian Inc., Wallingford CT*, 2010.

45 C. Lee, W. Yang and R. G. Parr, *Physical Review B*, 1988, **37**, 785.

46 C. Gonzalez and H. B. Schlegel, *The Journal of chemical physics*, 1989, **90**, 2154-2161.

47 C. Gonzalez and H. B. Schlegel, *The Journal of Physical Chemistry*, 1990, **94**, 5523-5527.

48 F. B. van Duijneveldt, J. G. van Duijneveldt-van de Rijdt and J. H. van Lenthe, *Chemical Reviews*, 1994, **94**, 1873-1885.

Figure Captions

Figure 1.Optimized structures of C_2H_2, HCl, un-doped $B_{12}N_{12}$ cluster(a), carbon-doped $B_{11}N_{12}C$(b) and $B_{12}N_{11}C$(c) cluster. Distances are in Å and angles are in °. Chlorine, carbon, boron, nitrogen and hydrogen atoms are depicted in blue-green, gray-green, pink, blue and silver-gray, respectively.

Figure 2.The calculated HOMO for $B_{12}N_{12}$(a), $B_{11}N_{12}C$(b) and $B_{12}N_{11}C$(c) at B3LYP/6-31+G** level. According to the introduction of carbon，the electrons redistribute on BN clusters and accumulate around the C1 atom in $B_{11}N_{12}C$, as well as for $B_{12}N_{11}C$. These figures will contribute to the prediction of adsorption cite.

Figure 3.The energy gaps of HOMO-LUMO between adsorbates(C_2H_2 and HCl) and BNC clusters are illustrate in this figure for intuitive understanding. Further detail data is provides in Table 1.

Figure 4.The adsorption energies of C_2H_2 and HCl separately adsorbed on BN clusters. We can easily conclude that the introduction of carbon on $B_{12}N_{12}$ could improve the ability of C_2H_2 and HCl adsorb on $B_{12}N_{12}$. (Energies in kcal·mol^{-1})

Figure 5.The first two structures are C_2H_2 and HCl physical adsorb on $B_{12}N_{12}$ cage. A, B and C are corresponding to the three most stable adsorption configurations of C_2H_2 adsorb on $B_{11}N_{12}C$ and $B_{12}N_{11}C$, respectively. All distances are in Å and angles are

in °. Chlorine, carbon, boron, nitrogen and hydrogen atoms are depicted in blue-green, gray-green, pink, blue and silver-gray, respectively.

Figure 6.The energy profiles for the different reaction pathways R1, R2 and R3 of acetylene hydrochlorination over the BNC ($B_{12-n}N_{11+n}C$(n=0,1)) cages. R1, R2 and R3 are separately start from adsorption complex A, B and C. (Energies in kcal·mol^{-1})

Figure 7.Optimized structures of stationary points for reaction channel R1. The blue arrow presents the direction of vibration of H1 atom. All distances are in Å and angles are in °.

Figure 8.Optimized structures of stationary points for reaction channel R2. It has the same De-ads and Pr state with R1.The blue arrow presents the direction of vibration of H1 atom. All distances are in Å and angles are in °.

Figure 9.Optimized structures of stationary points for reaction channel R3. The blue arrow presents the direction of vibration of H1 atom. All distances are in Å and angles are in °.

Figure 1

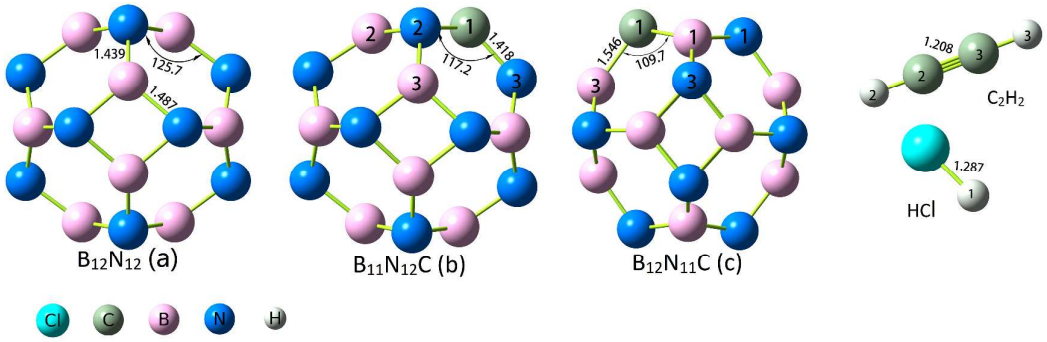

Figure 2

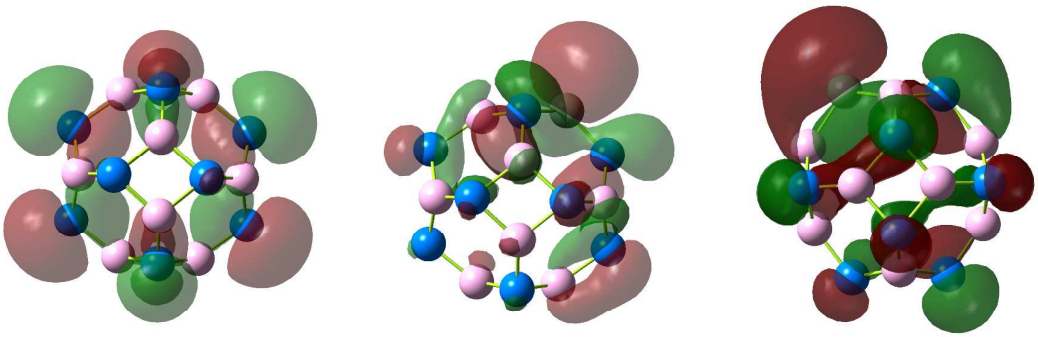

(a) (b) (c)

Figure 3

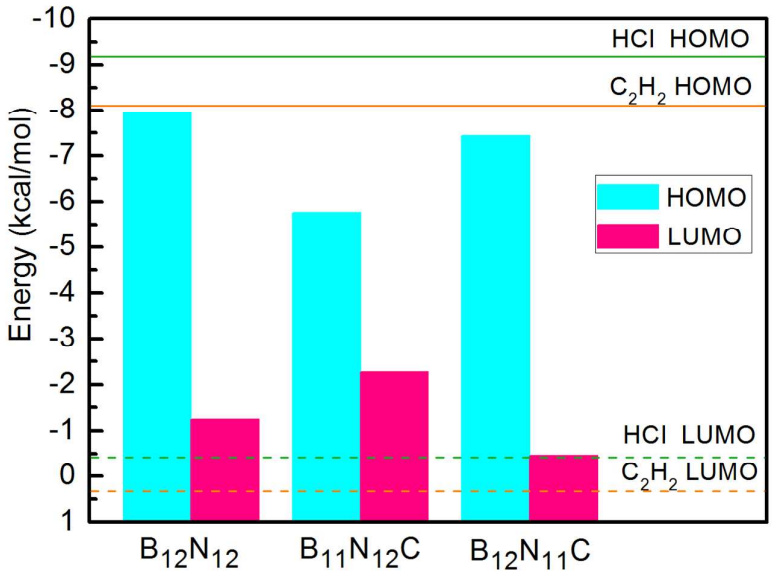

Figure 4

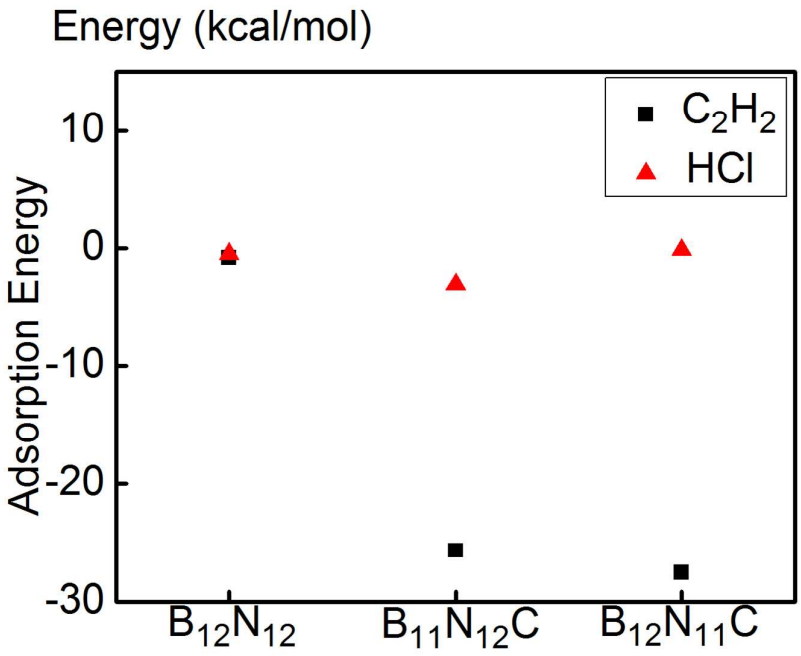

Figure 5

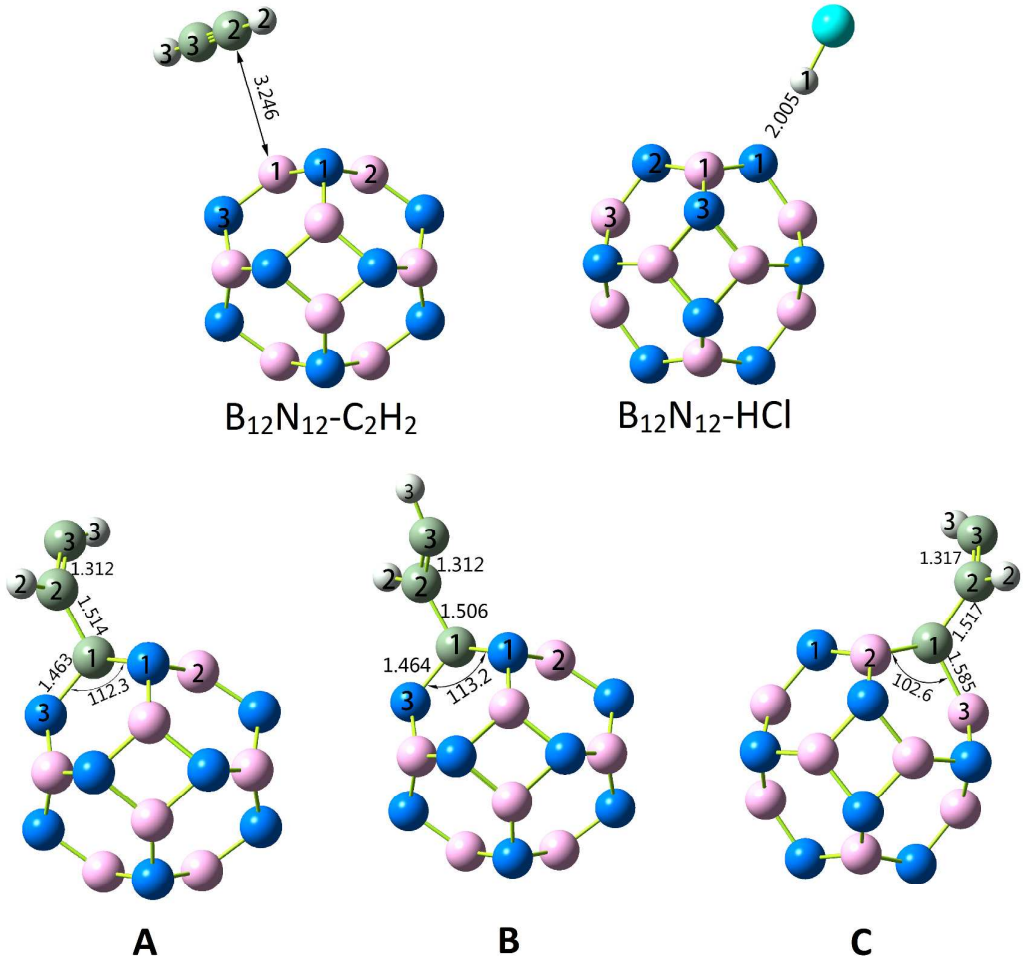

Figure 6

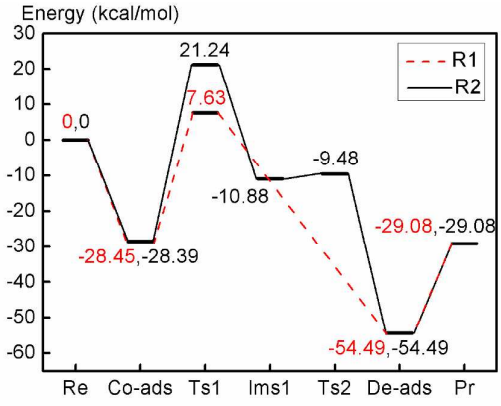

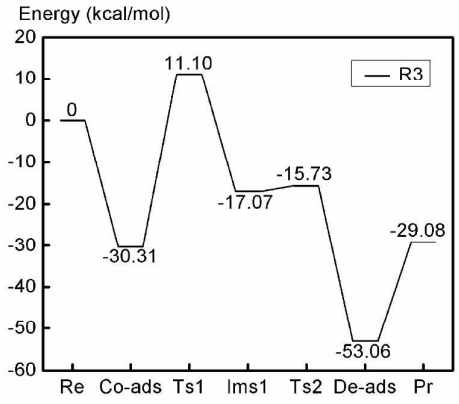

Figure 7

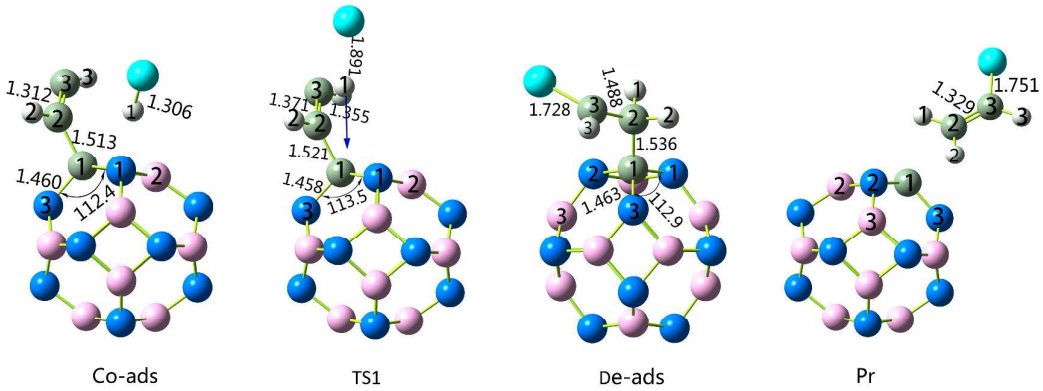

Figure 8

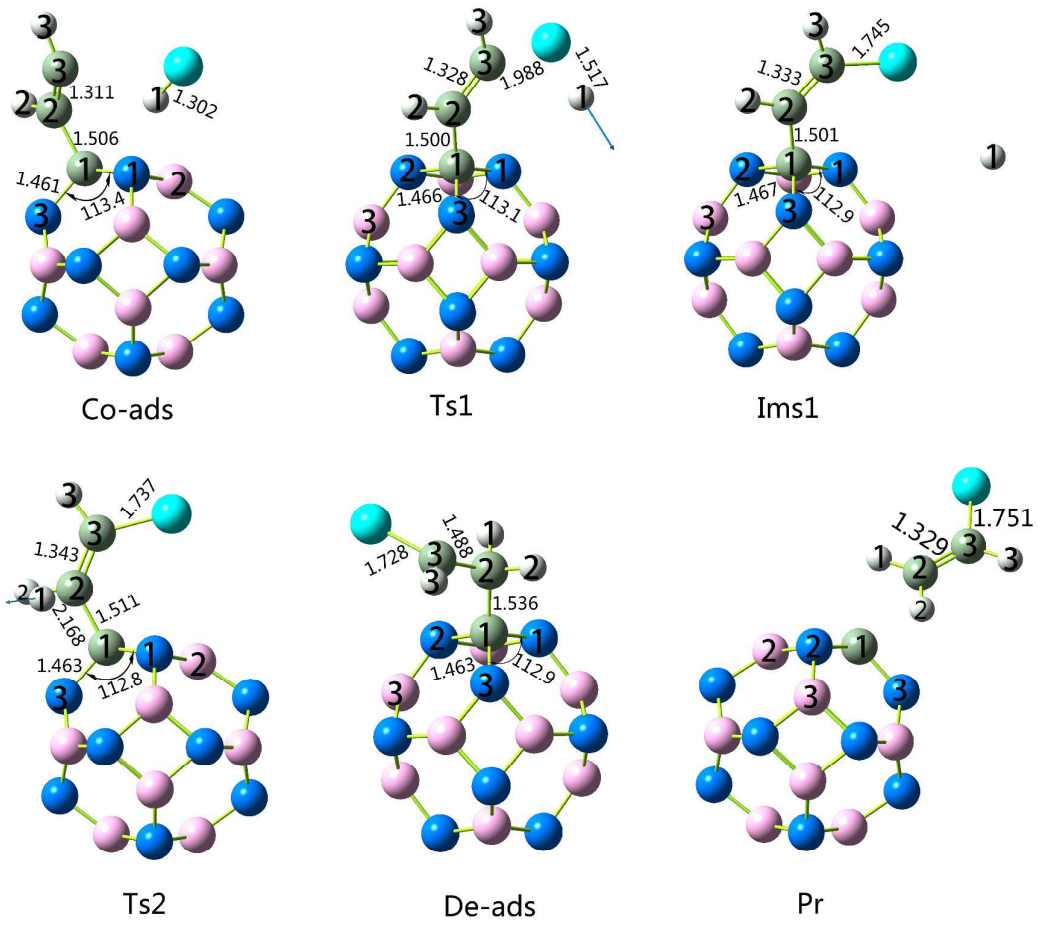

Figure 9

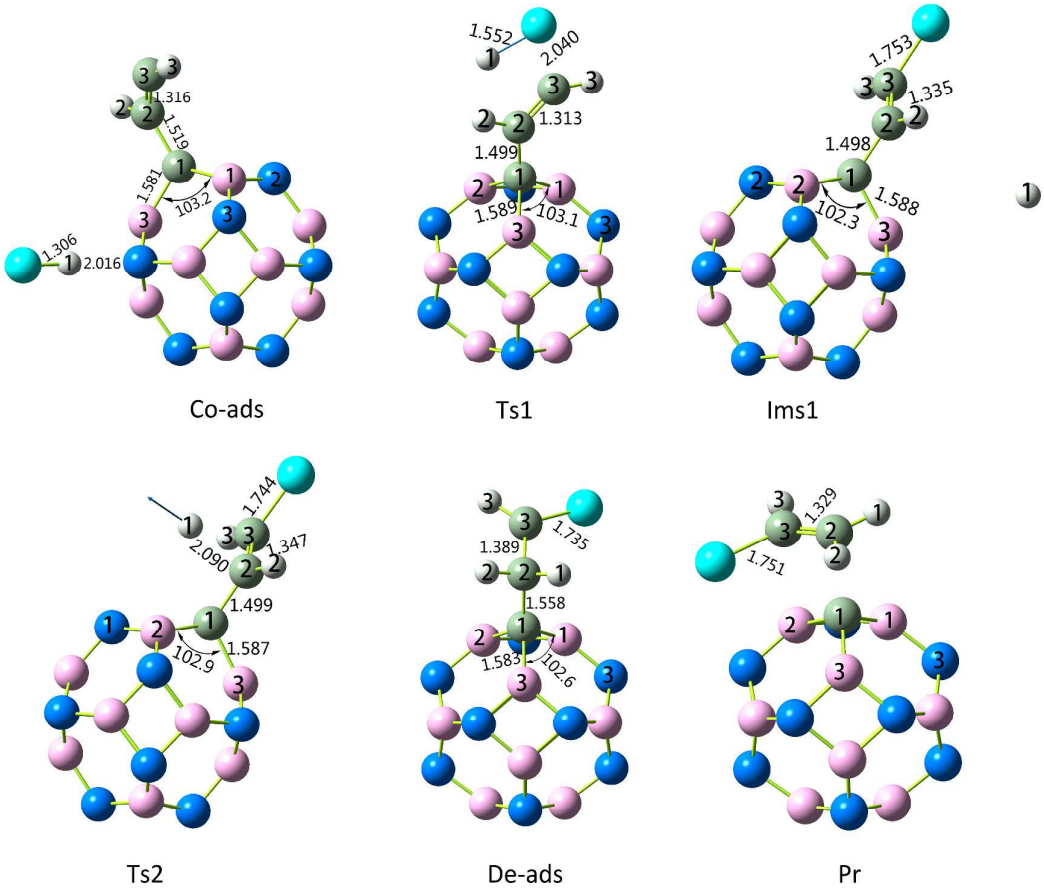

Table 1.The orbital energies on the HOMO and LUMO of C_2H_2, HCl, $B_{12}N_{12}$, $B_{11}N_{12}C$ and $B_{12}N_{11}C$, and their energy gaps between C_2H_2, HCl and BNC ($B_{12-n}N_{11+n}C$(n=0,1)) cages.(energies in eV, isovalue = 0.02)

			HOMO-LUMO (BNC→C_2H_2)	HOMO-LUMO (BNC→HCl)	HOMO-LUMO (C_2H_2/HCl→$B_{12}N_{12}$)	HOMO-LUMO (C_2H_2/HCl→$B_{11}N_{12}C$)	HOMO-LUMO (C_2H_2/HCl→$B_{12}N_{11}C$)
	HOMO	LUMO	C_2H_2	HCl	$B_{12}N_{12}$	$B_{11}N_{12}C$	$B_{12}N_{11}C$
C_2H_2	-8.08	0.35			6.84	5.81	7.62
HCl	-9.19	-0.42			7.95	6.92	8.73
$B_{12}N_{12}$	-7.95	-1.24	8.30	7.53			
$B_{11}N_{12}C$	-5.76	-2.27	6.11	5.34			
$B_{12}N_{11}C$	-7.43	-0.46	7.78	7.01			

Table 2.The optimal adsorption energies of C_2H_2 and HCl separately adsorb on BNC ($B_{12-n}N_{11+n}C(n=0,1)$) cages.(energies in kcal·mol^{-1})

	$B_{12}N_{12}$	$B_{11}N_{12}C$	$B_{12}N_{11}C$
C_2H_2	-0.79	-25.70	-27.58
HCl	-0.50	-3.06	-0.16

Table 3.Comparison of the energy barriers for acetylene hydrochlorination in rate-limiting step obtained with different catalysts (energies in kcal·mol^{-1})

Catalyst	Energy barrier(kcal/mol)	Ref.
$B_{11}N_{12}C$	36.08	This work(R1)
$AuCl_3$	11.86	30
g-C_3N_4/AC	77.94	39
PSAC-N	28.83	41
NCNT	32.52	42

Graphic for manuscript